Journal of Hazardous Materials 449 (2023) 131018

Contents lists available at ScienceDirect

Journal of Hazardous Materials

journal homepage: www.elsevier.com/locate/jhazmat

Research Article

Effect and mechanism of simultaneous cadmium-tetracycline removal by a self-assembled microbial-photocatalytic coupling system

Yu Wang [a], Hang Qiu [a], Huan Niu [a], Hao Liu [a], Jinchang Liu [a], Yinxue Jia [a], Haitao Ma [a], Fei Xu [b], Likai Hao [c], Zhongping Qiu [a,*], Can Wang [a,*]

[a] Sichuan Engineering Research Center for Biomimetic Synthesis of Natural Drugs, School of Life Science and Engineering, Southwest Jiaotong University, Chengdu 610031, Sichuan, PR China
[b] Key Laboratory of Bio-Resource and Eco-Environment of Ministry of Education, College of Life Sciences, Sichuan University, Chengdu 610065, Sichuan, PR China
[c] State Key Laboratory of Environmental Geochemistry, Institute of Geochemistry, Chinese Academy of Sciences, Guiyang 550081, PR China

HIGHLIGHTS

- *S. oneidensis* bio-recover Cd as CdS for visible light photocatalytic degradation.
- Self-assembled intimately coupled photocatalysis-biodegradation system (SA-ICPB).
- Photocatalysis and biodegradation efficiency is enhanced in the bio-hybrid system.
- SA-ICPB prefers aerobic conditions and works differently anaerobically.

GRAPHICAL ABSTRACT

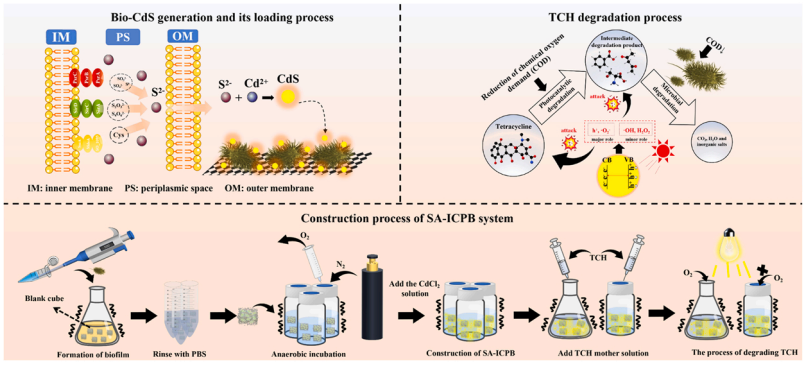

ARTICLE INFO

Editor: Jelena Radjenovic

Keywords:
Microbial-photocatalytic coupling
Bio-CdS
Self-assembling
Tetracycline hydrochloride
Degradation mechanism

ABSTRACT

Electrochemical bacteria *Shewanella oneidensis* MR-4 (MR-4) was used to biologically generate cadmium sulfide (bio-CdS) nanocrystals and construct a self-assembled intimately coupled photocatalysis-biodegradation system (SA-ICPB) to remove cadmium (Cd) and tetracycline hydrochloride (TCH) from wastewater. The characterization using EDS, TEM, XRD, XPS, and UV–vis confirmed the successful CdS bio-synthesis and its visible-light response capacity (520 nm). 98.4% of Cd^{2+} (2 mM) was removed during bio-CdS generation within 30 min. The electrochemical analysis confirmed the photoelectric response capability of the bio-CdS as well as its photocatalytic efficiency. Under visible light, SA-ICPB entirely eliminated TCH (30 mg/L). In 2 h, 87.2% and 43.0% of TCH were removed separately with and without oxygen. 55.7% more chemical oxygen demand (COD) was removed with oxygen participation, indicating the degradation intermediates elimination by SA-ICPB required oxygen participation. Biodegradation dominated the process under aerobic circumstances. Electron paramagnetic resonance analysis indicated that h^+ and $\cdot O_2^-$ played a decisive role in photocatalytic degradation. Mass spectrometry analysis proved that TCH was dehydrated, dealkylated, and ring-opened before mineralizing. In conclusion, MR-4 can spontaneously generate SA-ICPB and rapidly-deeply eliminate antibiotics by coupling

* Corresponding authors.
E-mail addresses: xufei@scu.edu.cn (F. Xu), haolikai@mail.gyig.ac.cn (L. Hao), zhpqiu@swjtu.edu.cn (Z. Qiu), wangcan@swjtu.edu.cn (C. Wang).

https://doi.org/10.1016/j.jhazmat.2023.131018
Received 7 December 2022; Received in revised form 4 February 2023; Accepted 15 February 2023
Available online 16 February 2023

photocatalytic and microbial degradation. Such an approach was efficient for the deep degradation of persistent organic pollutants with antimicrobial properties.

Nomenclature

TCH	Tetracycline hydrochloride
COD	Chemical oxygen demand
HMs	Heavy metals
Cys	Cysteine
AOPs	Advanced oxidation processes
ROS	Reactive oxygen species
EPS	Extracellular polymeric substances
Bio-CdS	Biologically produced cadmium sulide
LD	Light degradation
PA	Physical adsorption
PT	Photocatalysis treatment
BD	Biodegradation
BA	Biological Adsorption
BT	Biological treatment
PD	Photocatalytic degradation
SA-ICPB	Self-assembled intimately coupled photocatalysis and biodegradation
EET	Extracellular electron transport

1. Introduction

The widespread of antibiotics and heavy metals (HMs) has led to severe risks to the ecosystem and human health [5,24]. Antibiotics and HMs have been widely used in the livestock industry to treat animal infections, prevent disease, and promote growth [22]. The global veterinary antibiotics consumption reached 93,309 tons in 2017 and is expected to reach 105,596 tons by 2030 [40]. However, 60–90% of veterinary antibiotics and 80–90% of HMs additives are excreted into the environment along with animal feces and urine [13], causing serious ecological risks [14]. HMs concentration in livestock waste in Shanxi, China, reached 2153.9–2755.2 mg/kg [11], while tetracycline (TCH) in livestock sludge in Heilongjiang, China, was as high as 30.5–388.70 ug/kg [43]. As a result, HMs and antibiotics coexist in the husbandry wastewater, causing severe concerns about the combined contamination [58].

Numerous physical and chemical methods have been used to treat polluted wastewater, such as redox, adsorption, ion exchange, and advanced oxidation processes (AOPs) [36,52,57]. Recently, the intimately coupled photocatalysis and biodegradation (ICPB) methods have been used to remove a variety of organic pollutants such as chlorophenols [44], polycyclic aromatic hydrocarbons [35], and antibiotics [9,50]. In an ICPB, the porous carrier surface supports the photocatalyst, while the inner layer is used to load microorganisms. ICPB combines the advantages of photocatalytic and biological degradation. ROS generated by photocatalysis cracks refractory pollutants with antimicrobial properties that microorganisms cannot utilize [31]. The biodegradable intermediates are transported to microorganisms rapidly to achieve deep degradation due to the close adjunction of microorganisms and photocatalysts. Compared with traditional photocatalysis, ICPB is less prone to accumulate photocatalytic products, which can be readily eliminated by coupled biodegradation [61].

However, there are some challenges. Most ICPB systems target a single pollutant, while multiple pollutants coexist in actual contaminated sites, which may decrease microbial metabolic activity and reduce system efficiency. Besides, constructing ICPB requires artificial synthesis and loading of photocatalysts, involving many organic reagents and sophisticated processing. The process is easy to cause secondary pollution and cannot remove or recover HMs in sewage. These shortcomings limit the cost-effective and environmentally safe operation of ICPB. Naturally, using microorganisms to generate photocatalysts and self-assemble a microbial-photocatalysis system is in thought. Microorganisms can use the polysulfide compounds in wastewater to biosynthesis sulfides [10,37]. For example, *Shewanella oneidensis* can convert polysulfide compounds into S^{2-} through various pathways (SirACD、PsrABC、MdeA、SO_1095, and SseA) to achieve HMs recovery as sulfides (e.g., CdS) [46]. The process avoids the chemical synthesis and adoption of photocatalysts and recovers HMs for further use.

Based on the above facts, this study constructed a self-assembled intimately coupled photocatalysis and biodegradation system (SA-ICPB) using *Shewanella oneidensis* MR-4 to remove Cd and TCH simultaneously. Bio-generated CdS nanoparticles (Bio-CdS) and bacteria cells coexisted on a porous carrier to combine photocatalysis with biodegradation. Multi techniques were applied to characterize the morphology and verify the potency. Besides evaluating pollutants removal efficiency, electrochemical analysis, electron paramagnetic resonance, and mass spectra were used to speculate the potential degradation pathways and mechanisms. The results support the feasibility of the SA-ICPB and the potential for synchronous removal of HMs and antibiotics. The current research is expected to provide a novel approach for the depth treatment of contaminated wastewater, which also gives a new perspective on combining chemical and biological techniques in the environmental field.

2. Material and methods

2.1. Bacteria cultivation and CdS biosynthesis

The electrochemical bacteria *Shewanella oneidensis* MR-4 (MR-4) was used to construct a self-assembled intimately coupled photocatalysis and biodegradation (SA-ICPB) system. The strain was obtained from Dr. Likai Hao of the Institute of Geochemistry, Chinese Academy of Sciences (Strain number: CICC 25104 and NCBI sequence number: NC_008321.1). For cultivation, the bacteria were added to LB medium and incubated at 200 rpm/min at 30 °C for 12 h, centrifuged at 6000 rpm for 6 min, and the collected bacterial cells were washed with PBS buffer (Table S3) 3 times [1]. Then the initial optical density of 0.52 (OD 600, 4~6 × 10^6 CFU/mL) was adjusted and suspended in 50 mL inorganic salt medium (Table S1). The bacterial suspension was added to a 100 mL serum bottle and bubbled with high-purity nitrogen for 10 min. The serum bottles were sealed with aluminum caps with a butyls rubber stopper and incubated in a shaker (30 °C, 200 rpm/min) for 12 h. Then 2 mM $CdCl_2$ was added [48]. The cultivation continued for 24 h, and the yellow precipitate at the bottom was collected by centrifugation at 6000 rpm for 6 min later. The precipitate (biogenerated CdS, bio-CdS) was rinsed twice with PBS and fixed with 2.5% glutaraldehyde for 6 h at 4 °C.

After gradient dehydration with ethanol, CO_2 critical point drying, and gold spraying, the morphology and elemental composition of bio-CdS were analyzed using a scanning electron microscope (SEM, ZEISS GeminiSEM 300, Germany) with energy dispersive spectroscopy (EDS) [49]. The extracellular distribution and lattice fringe patterns were analyzed by transmission electron microscopy (TEM, JEOL JEM 2100 F, Japan) [15]. An X-ray powder diffraction spectrometer (XRD, Thermo Scientific K-Alpha, USA) was also used to validate the crystal structures. The valence changes of Cd and S in the bio-CdS were determined by X-ray photoelectron spectroscopy (XPS, Thermo VG Scientific, ESCALAB 250, USA). In addition, the UV–visible diffuse reflectance spectrum (UV–vis DRS, Shimadzu UV-3600I Plus, Japan) was used to determine

the optical absorption properties. A steady/Transient State Fluorescence Spectrometer (PL, Edinburgh FLS-980, UK) was used to determine the separation and recombination ability of photogenerated electrons and holes of bio-CdS [42].

2.2. System Construction

Sterile polyurethane sponge cubes from Aiqin Environmental Protection Co. LLC., Wuxi, China (dimensions 1 cm × 1 cm×1 cm, 90% porosity) were used as a carrier to construct SA-ICPB. The cubes were immersed in an LB medium of MR-4 to load the bacterial cell. The medium was replaced every 3 days for 7 days. Then the cubes were removed and washed with sterile water twice to remove the residual medium. The loaded sponge cube was transferred into a 100 mL serum bottle containing 50 mL inorganic salt medium with 5 mM cysteine. The bottles were bubbled with high-purity nitrogen for 10 min to eliminate oxygen. Then, the serum bottles were sealed with aluminum caps with butyl rubber stoppers and placed in a shaker (30 °C, 200 rpm/min) for 12 h before adding 2 mM $CdCl_2$.

During SA-ICPB assembly, Cd^{2+} was removed due to bio-precipitation. The following groups were set to investigate the removal process: SA-ICPB, as described above; Physical Adsorption (PA), using the unloading sponge to remove Cd^{2+}; Biological Adsorption (BA), using the bacteria cell to remove the Cd^{2+}. The atomic absorption spectrometer (PinAAcle900T, USA) measured the Cd^{2+} concentration at 0, 30, 60, 120, 240, and 480 min

2.3. Effect evaluation of the system

2.3.1. TCH and COD elimination

After construction, 5 g/L TCH ($C_{22}H_{24}N_2O_8$ HCl, 98%, Sigma-Aldrich Co.LLC., USA) was added to reach 30 mg/L TCH in the medium. Then the pollutants removal test was conducted (120 rpm, 28 °C). Besides SA-ICPB, the following groups were set to investigate the pollutants removal mechanism. Light Degradation (LD): only use visible light to test TCH removal by photolysis; Physical adsorption (PA): only use the sponge carrier to test TCH removal by adsorption (dark); Biodegradation (BD): only use the bacteria cell to test TCH removal by biological effect (dark); Photocatalytic degradation (PD): only use bio-CdS to test TCH removal by photocatalytic effect under visible light, the bacteria were inactivated. Besides, the influence of oxygen was considered to explore the effect of microbial and photocatalysis degradation (bio-CdS). The LED lamp board provides visible light, and the optical density is adjusted to 5.38×10^{-5} einstein/(L·s). TCH concentrations (2, 4, 6, 8, 12 h) were determined using an Agilent 1290 HPLC with a 4.6 × 50 mm, 5 μm wondasil C18 column. The column temperature was 30 °C, and the wavelength of the ultraviolet (UV) detector was set to 355 nm. The mobile phase consisted of 0.01 M oxalic acid (76%, v/v), acetonitrile (16%), and methanol (8%) at a flow rate of 1.0 mL/min. Chemical oxygen demand (COD) was determined using commercial reagents according to the protocal (Hach Company, Loveland, CO) [6].

2.3.2. Degradation process and mechanism

The degradation intermediates of TCH were analyzed by Agilent LC1290-QQQ-6470 liquid chromatography-mass spectrometry (LC-MS). The mobile phase consisted of 20% (v/v) acetonitrile and 80% 0.1% formic acid in water at a flow rate of 0.35 mL/min. The injection volume was 10 μL, and the column temperature was 30 °C. MS was performed in positive ion mode using ESI under the following conditions: capillary voltage 3500 V, cone voltage 29 V, source temperature 150 °C, solvent removal temperature 350 °C, conical gas flow rate 50 L/h, and gas flow rate 600 L/h. The scanning mass range is 50–1000 *m/z*. To study the photocatalytic degradation, the hydroxyl radical scavenger (tert-butanol, TBA), the superoxide radical scavengers (p-benzoquinone, p-BQ) and the hole sacrificial agent (ammonium oxalate, AO) were introduced [47]. An electron paramagnetic resonance spectrometer (EPR/ESR, Bruker A300, Germany) was also used to measure the free radicals in the reaction process, where DMPO and TEMPO were used as free radical trapping agents [7].

2.4. Electrochemical analysis of the system

Electrochemical tests were conducted to study electron transport at the microbial-photocatalyst interface. An electrochemical workstation (Ch660e, Shanghai Chenhua Instrument Co., Ltd., Shanghai, China) with a three-electrode system was employed. Working electrode, 1 × 1 cm^2 stainless steel mesh; Counter electrode: a platinum sheet; Reference electrode: Ag/AgCl saturated electrode; Electrolyte: 0.1 M PBS. The dissolved oxygen was removed by bubbling with high-purity nitrogen for 15 min before use. The surface of the electrolytic cell is wrapped with tin foil to simulate the dark environment. However, a window is left on the side of the working electrode to test the photovoltaic effect.

The following groups were set: SA-ICPB (working electrode loaded with biofilm and bio-CdS), BT (biological treatment, working electrode loaded with biofilm), PT (photocatalysis treatment, working electrode loaded with bio-CdS), and Blank as control. Cyclic voltammetry (CV) was conducted to detect the electron transfer at the interface of electrodes. The instantaneous photocurrent response (TPC) was also measured by the timed current method to evaluate the photogenerated electron-hole separation in the photoelectrode. Linear scanning voltammetry (LSV) was used to measure the linear change of current with voltage in different systems within a specific range of electric potential windows, which was used to evaluate the electron transfer ability [9].

2.5. Statistical analysis

All the tests were performed in triplicates (n = 3). The experimental data were evaluated with a one-way analysis of variance (ANOVA) to calculate the mean and standard deviation values using the SPSS package (version 21.0). Moreover, the mean values were compared based on Fisher's least significant difference (LSD) procedure at a significance level of $P < 0.05$. All the figures were plotted with Origin 2021 software.

3. Results and discussion

3.1. Characterization of bio-CdS

Before the bio-generation, the media was transparent, with the white sponge cube floating inside. However, the metabolism of MR-4 generated a large amount of yellow substance on the carrier and in the media (Fig. 1a). After bio-generation, a single cube was loaded with about 2.2 mg product (Fig. S2a). The SEM result indicated that the biosynthesized nanoparticles were uniformly distributed on the bacteria and the carrier surface, with size mainly between 40 and 50 nm (Fig. 1b). Although small aggregates sparsely presented outside the cell, no large spherical aggregates were formed. Fig. 1c shows the presence of microbial nanowires, which may contribute to the microbial extracellular electron transport (EET) process. TEM (Fig. 1d-e) showed that the nanoparticles were tightly attached to the cells, and their actual size may be smaller. However, due to the inevitable adsorption of extracellular polymeric substances (EPS) [2], bio-CdS were stacked to form small CdS aggregates, which was consistent with the SEM results. HRTEM image (Fig. 1f) showed the crystal plane spacing of bio-CdS (0.34, 0.29, and 0.175 nm) is in good agreement with (111), (220), and (311) of hawleyite. The EDS surface scanning map (Fig. 1g-i) showed that the nanoparticle's atomic ratio of Cd and S was about 1:1.

The XRD analysis (Fig. 2a) matched the three most substantial peaks at 26.51°, 43.96°, and 52.13°. The corresponding lattice surfaces were (111), (220), and (311), which corresponded to the crystal planes of hawleyite (JCPDS, 10–0454). The results were consistent with the HRTEM image (Fig. 1c). XPS spectra (Fig. 2b-d) showed that Cd $3d_{5/2}$ (404.80 eV) and Cd $3d_{3/2}$ (411.60 eV) have similar binding energies

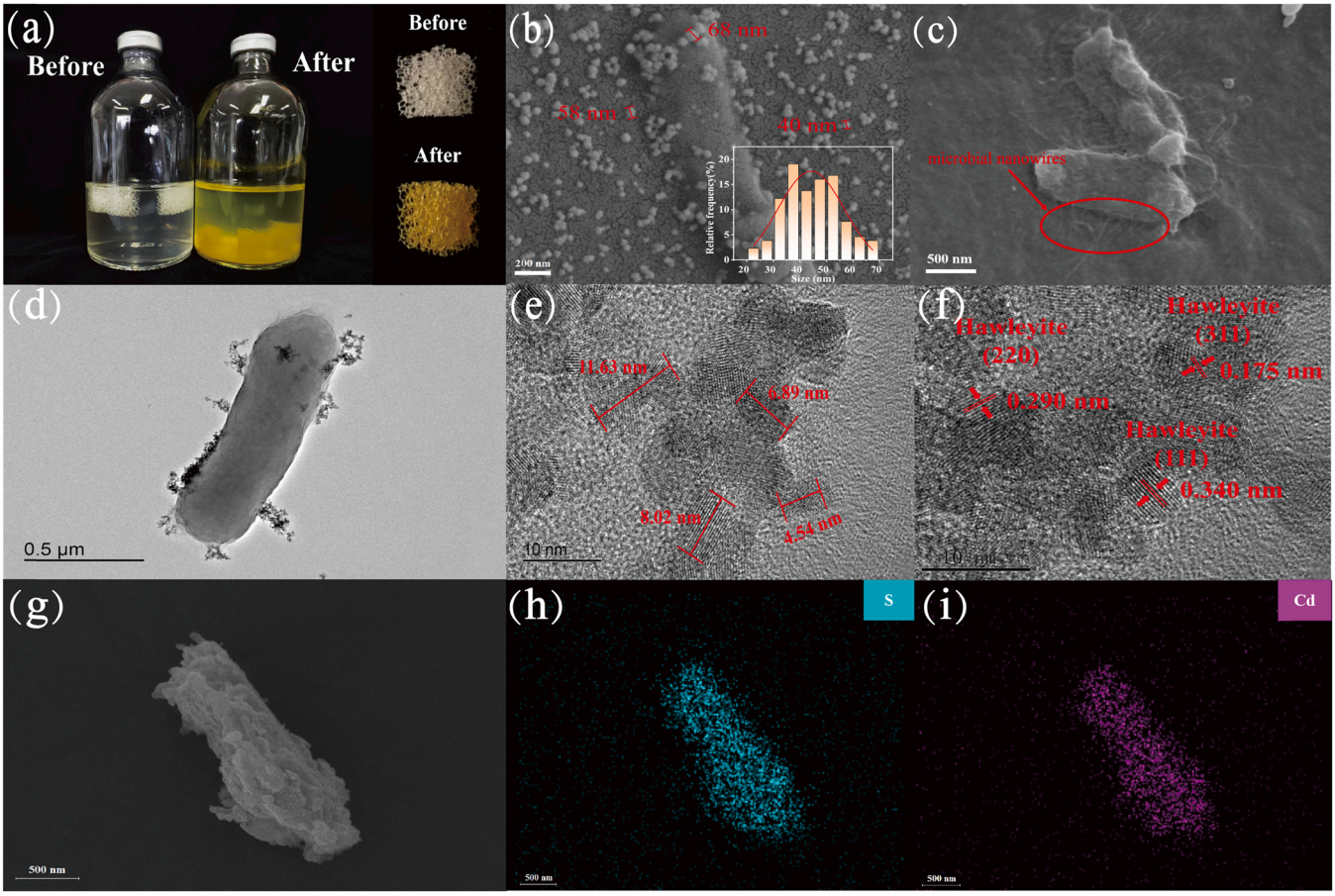

Fig. 1. (a) Before and after the construction of self-assembled ICPB (SA-ICPB) system. (b) SEM images of polyurethane sponge carrier incubated for 12 h (inset: histograms of the particle size distribution of bio-CdS); (c) Microbial nanowires on the surface of bacteria. (d) STEM image of microorganism and bio-CdS nanoparticles. (e) Dimensions of bio-CdS in STEM images. (f) HRTEM image of bio-CdS; (g-i) EDS surface scanning results of microbial coated CdS nanoparticles.

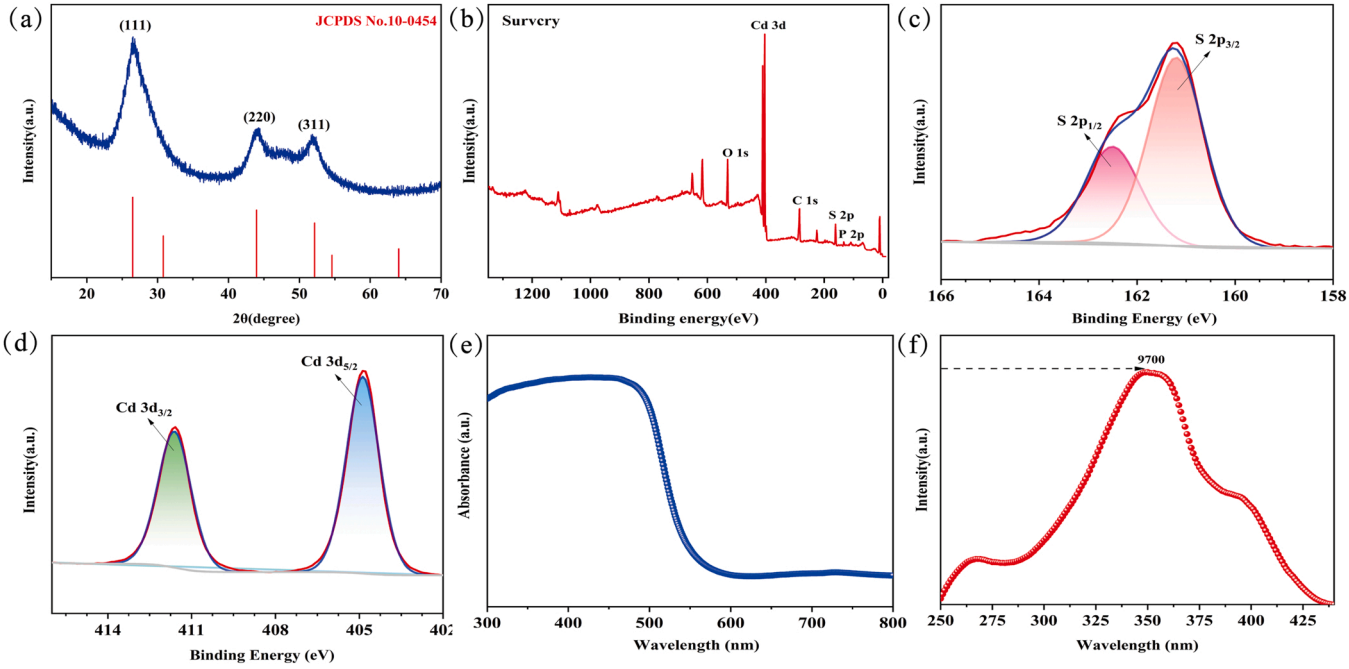

Fig. 2. (a) XRD spectrum of the bio-CdS. (b-d) XPS spectrum of the bio-CdS. (e) UV–vis diffuse reflection spectrum of bio-CdS. (f) PL excitation spectrum of bio-CdS.

compared to the standard Cd $3d_{5/2}$ (405.10 eV) and Cd $3d_{3/2}$ (411.70 eV), indicating a clear Cd^{2+} signal. The S 2 P orbital also showed an obvious S^{2-} signal. The above result confirmed the successful biosynthesis of CdS. By UV–vis DRS (Fig. 2e), the product showed a strong absorption at 520 nm with a direct bandgap energy of 2.28 eV (Fig. S2c). Compared with chemically synthesized CdS, the bio-CdS has a smaller band gap, positively affecting the photocatalytic reaction [23]. CdS have an E_{VB} and E_{CB} of 1.67 eV and − 0.58 eV, respectively [41]. With an E_{VB} lower than 1.99 eV, CdS cannot oxidize the H_2O and generate·OH. However, with an E_{CB} lower than − 0.33 eV, CdS can reduce O_2 and generate·O_2^-, contributing to the degradation of pollutants [27].

By PL analysis (Fig. 2f), the bio-CdS showed a decreased fluorescence intensity compared with chemically generated CdS (Fig. S2d). Fluorescence intensity indicated the recombination efficiency of electrons and holes separated under light irradiation [16]. The relatively lower fluorescence emission indicated the slowed photogenerated electron-holes recombination and higher light energy utility efficiency and photocatalytic activity of the bio-CdS, probably due to the structural difference [23].

3.2. Evaluation of pollutant removal

During SA-ICPB construction, Cd^{2+} was removed due to adsorption by the carrier, adsorption/accumulation by the bacteria, and coprecipitation as CdS. With an initial Cd^{2+} at 2 mM, Cd^{2+} removal in the SA-ICPB group reached 98.52% in 30 min (Fig. 3a), which was far higher than biological adsorption (BA, 10.17%) and physical adsorption (PA, 23.67%). The results indicated coprecipitation as CdS was the main route for Cd^{2+} removal [17] and constructing SA-ICPB efficiently recovered HMs resources from wastewater [38].

Fig. 3b-d presented the dynamic removal of TCH and COD. Physical adsorption (PA) removed 39.6% and 28.3% of TCH under aerobic and anaerobic conditions in 12 h, respectively. The result indicated that the carrier adsorption and natural oxidation slightly contributed to TCH removal [4]. Biological degradation (BD) removed 84.3% and 12.6% of TCH under aerobic and anaerobic conditions. With oxygen as the electron acceptor, MR-4 can degrade TCH more efficiently. Without oxygen and other electron acceptors (e.g., ferric iron), the growth and metabolism of MR-4 become slower, and bacteria biosorption could be the main contributor to TCH removal [3]. However, the metabolism of MR-4 was vigorous under aerobic conditions, and TCH removal was caused by biosorption and biodegradation, with biodegradation playing a major role. As described in Fig. 3d, BD showed a similar COD removal efficiency with or without oxygen supply ($P > 0.05$), although more TCH was removed aerobically. Previous reports have documented that the biodegradation of antibiotics such as TCH could be hard and incomplete [8]. Therefore, high-level COD resided, which was an obstacle to the biological treatment of such complex organics.

The light degradation (LD) and the photocatalysis degradation (PD) also removed a certain amount of TCH. The photodegradation property of TCH could be responsible for the removal, leaving high-level intermediates and COD retention [34]. However, PD removed 71.22% and

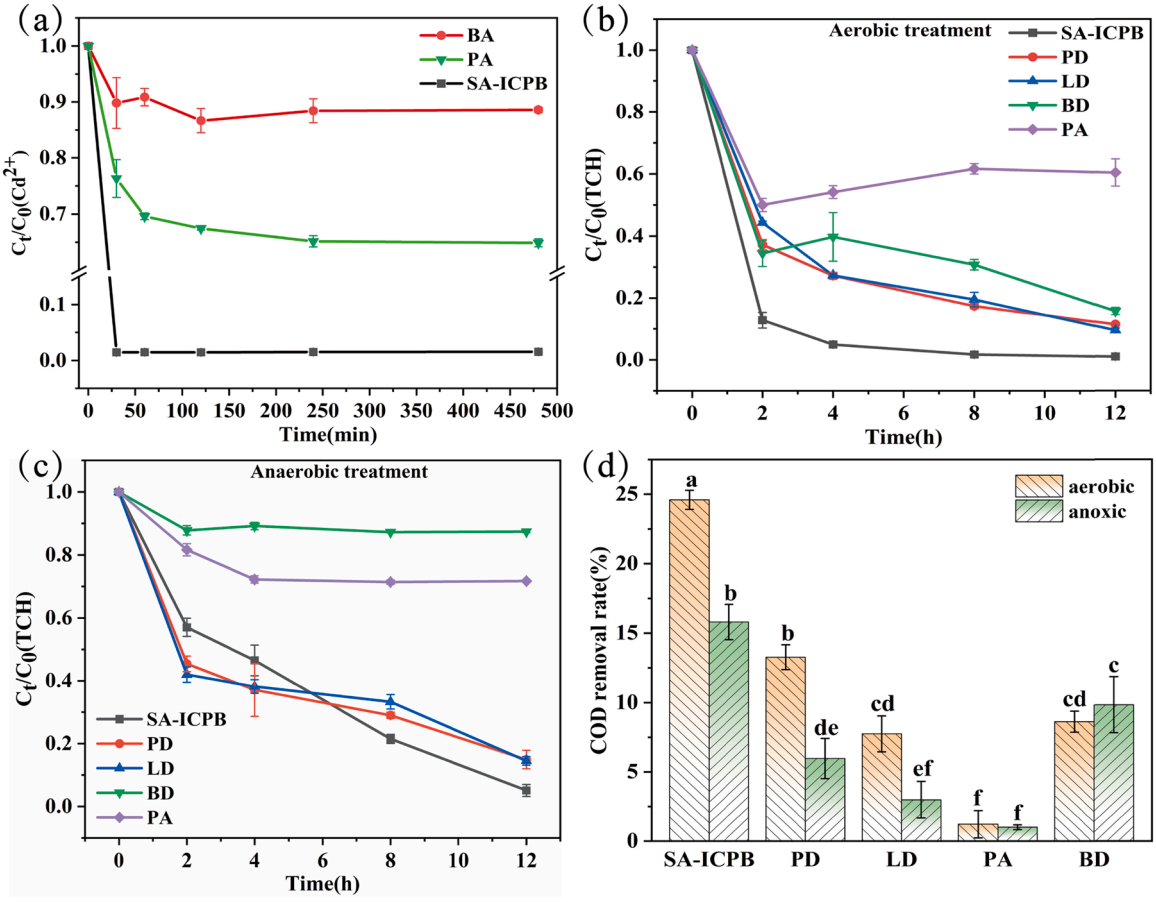

Fig. 3. (a) Heavy metal removal during SA-ICPB construction. (b) Antibiotic removal under aerobic conditions. (c) Antibiotic removal under anaerobic conditions. (d) COD removal under aerobic and anaerobic conditions. Note: In Fig. 3a, SA-ICPB, self-assembled intimately coupled photocatalysis and biodegradation system; Physical Adsorption (PA), using the unloading sponge to remove Cd^{2+}; Biological Adsorption (BA), using the bacteria cell to remove the Cd^{2+}. In Fig. 3b-d, SA-ICPB was used as the experimental group; Light Degradation (LD), under visible light without carrier or bacteria to investigate the effect of photolysis; Physical Adsorption (PA), to test the adsorption effect of the carrier under darkness; Biological Degradation (BD), considered TCH removal by bacteria, without carrier or light; Photocatalytic Degradation (PD), to test the effect of photocatalysis under visible light and the bacteria were inactivated.

99.66% more COD than LD, with and without oxygen, respectively. The result indicated that photocatalysis contributed significantly to TCH degradation, while single light degradation merely cracked or transformed the molecule [12]. SA-ICPB showed the highest pollutants removal, which removed 8.50–59.40% more TCH and 11.33–23.98% more COD than others aerobically, 9.40–82.30% more TCH and 5.97–14.83% more COD than others anaerobically. SA-ICPB functioned much better with oxygen and eliminated TCH entirely in 12 h. Notably, SA-ICPB removed 87.20% of TCH in 2 h aerobically but only 43.0% of TCH anaerobically. The result indicated that SA-ICPB could rapidly and profoundly degrade antibiotics, but the metabolism and respiration of the biofilm (MR-4) required oxygen as the electron acceptor.

Antibiotics could inhibit single biodegradation and reduce efficiency. While photocatalytic degradation is incomplete and prone to generating possibly toxic intermediates [20]. The synergistic photocatalysis and biodegradation in SA-ICPB overcome the shortcomings [25]. Photocatalysis readily broke down the ring-shaped molecule, leaving intermediates with simple structures and higher biodegradability for microbial metabolism. Biodegradation rapidly eliminated these photocatalytic products and avoided their competition for free radicals. Thus, the free radicals from photocatalysis react more readily with TCH, speeding up the reaction [45].

To investigate sustainability, 5 cycles of repetitive experiments were conducted (Fig. S3). After cycling, the TCH removal rate by SA-ICPB decreased slightly but was still above 90%. However, the removal of COD increased. The falling of bio-CdS from the carrier and the shielding of bacteria biofilm could have decreased photocatalysis efficiency and TCH removal. Nevertheless, the bacterial biofilm continuously grows and becomes more stable, which can degrade TCH and intermediate more efficiently, resulting in better COD elimination. In conclusion, the result indicated that SA-ICPB could perform efficiently under cycling conditions.

3.3. Photocatalytic mechanism of the bio-CdS

Employing ROS quenching experiment and the ESR analysis, the effect of photoinduced active substances was investigated (Fig. 4). The photocatalytic degradation of TCH by bio-CdS was significantly inhibited by the h^+ scavenger AO and O_2^- scavenger p-BQ by 26.23% and 16.35%, separately. However, the inhibition of ·OH scavenger TBA was limited (10.80%). The phenomenon indicated that·O_2^- and h^+ played a major role in TCH degradation, while the contribution of ·OH was minor, consistent with previous reports [51,59]. Fig. 4b revealed the second-order kinetics equation of photocatalytic degradation of TCH by SA-ICPB with or without scavenger (expressed as a linear fit of $1/C_t \sim t$, where C_t is TCH concentration at a given time). The k value in SA-ICPB was higher than that with a scavenger. AO and p-BQ significantly reduced the k value, while the influence of TBA was minimal. The ESR analysis (Fig. 4c) also showed a far stronger signal of ·O_2^- and h^+ than·OH and H_2O_2. The above result indicated that h^+ and ·O_2^- played a crucial role in the photocatalysis process, while the effect of H_2O_2 and ·OH were negligible [53,56]. Under visible light irradiation, the photogenerated electrons of bio-CdS are easily transferred to the conduction band (CB), while the h^+ accumulates on the valence band (VB), leading to effective charge separation. Thus, the electrons accumulated on CB can reduce O_2 to ·O_2^-, which oxidizes the organic molecules with the h^+ on VB [60].

3.4. Electrochemical analysis

Fig. 5 presented the CV and LSV curves of SA-ICPB with or without light radiation. The balk electrode showed no prominent redox peak (Fig. 5a). However, a reduction peak of − 310 mV (E_{Pc}) and an oxidation peak of − 115 mV (E_{Pa}) were observed when the bacteria were loaded (Fig. 5a), which may be caused by the EET via cytochrome C in the cell membrane [32]. The CV curves of the blank and BT showed no difference under light or darkness (not shown in the figure). Notably, no prominent redox peak was found in PT with or without illumination (Fig. 5b), indicating bio-CdS won't influence the electrochemical response of other constituents in SA-ICPB (e.g., bacteria cell).

Fig. 5c shows the electrochemical response of SA-ICPB. Under darkness, prominent redox peaks were observed at − 155 mV (oxidation peak) and − 310 mV (reduction peak). Compared with BT, the peak current of SA-ICPB under dark decreased, probably due to the coating and resistance of bio-CdS. Under the light, the current intensity of SA-ICPB increased, and the oxidation and reduction peak positions shifted. The phenomenon could be caused by the separation of electron-hole pairs generated by bio-CdS under light excitation. The bacteria-produced electrons may combine with holes, thus accelerating the EET process [54]. Therefore, the enhanced pollutants removal efficiency of SA-ICPB.

Fig. 5d shows the instantaneous photocurrent test of each treatment under no bias voltage. When bio-CdS (PT) was illuminated, the photogenerated electron-hole pair was separated, generating an instantaneous photocurrent. The current returned to zero immediately after the light source was turned off, indicating that the current was generated entirely by photoexcitation. Nevertheless, the current peak dropped quickly during the light period, indicating fast recombination of photogenerated electron-hole pairs, which could adversely affect photocatalytic efficiency [18]. However, no such phenomenon was observed when bio-CdS was loaded with microorganisms (SA-ICPB), indicating a positive effect of microorganisms in slowing the photogen-hole recombination. The lower photocurrent of SA-ICPB than PT was due to biofilm obstructing the light to photocatalysts [9].

To further confirm the electronic interaction between CdS and microorganisms in SA-ICPB, an LSV test was performed (Fig. 5e). In the dark, SA-ICPB showed higher current strength than PT and BT, which was consistent with the CV curve. Under the light condition, the

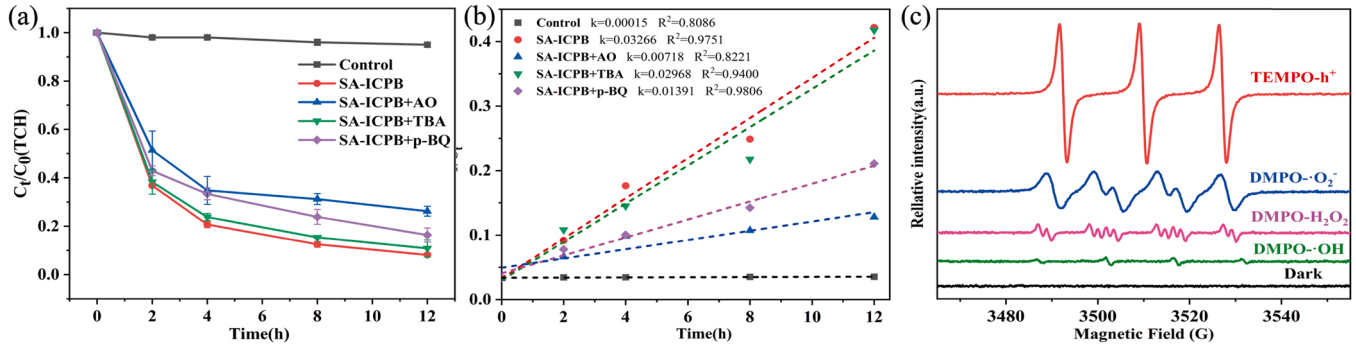

Fig. 4. (a) Free radical trapping experiment of SA-ICPB. (b) Fitting curves of the corresponding $1/C_t$ second-order reaction kinetics with time. (c) ESR spectra of bio-CdS materials.

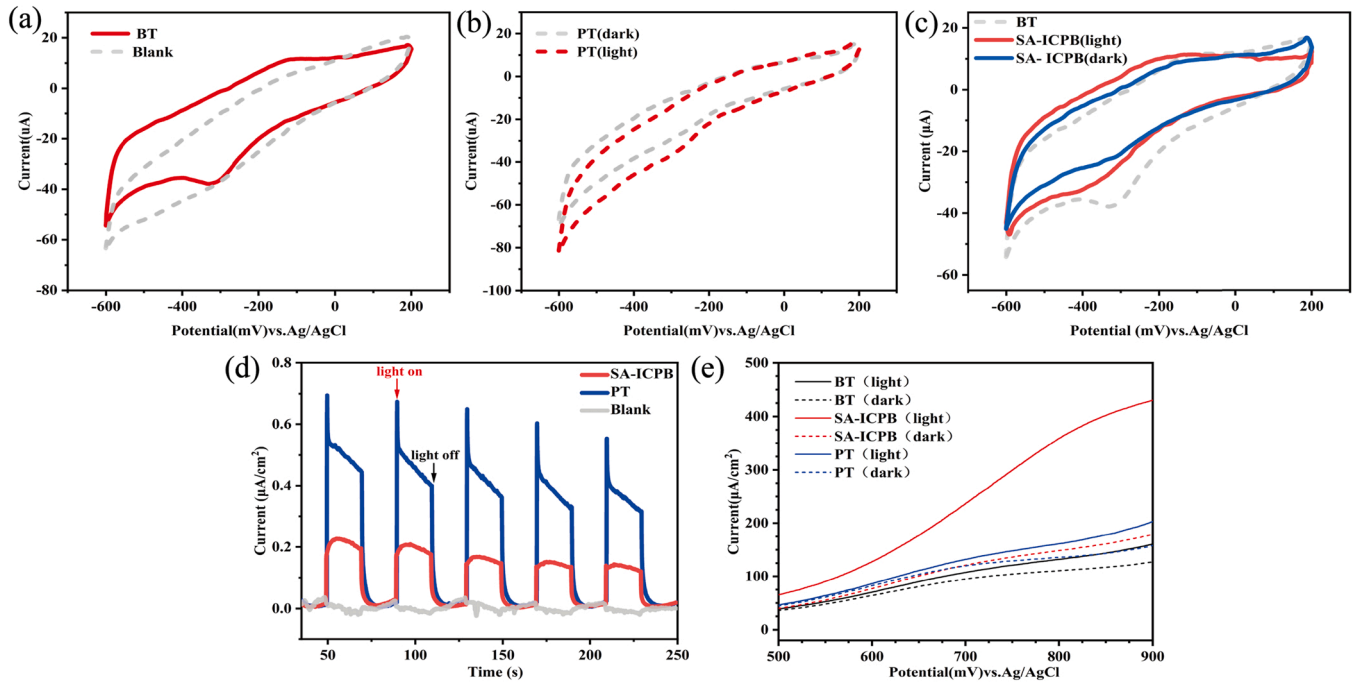

Fig. 5. (a) CV curves of working electrode loaded with bio-CdS (PT) under light/dark. (b) CV curves of the blank working electrode (Blank) and electrode loaded with *S. oneidensis* MR-4 (BT). (c) CV curves of working electrode loaded with CdS and MR-4 (SA-ICPB) under light/dark. (d) Instantaneous photocurrent testing of SA-ICPB and PT. (e) LSV curves under light/dark.

photocurrent gradually increased with electrode potential. At 0.9 V, the SA-ICPB and PT produced 430.5 μA/cm^2 and 203.1 μA/cm^2 photocurrents, respectively. The result indicated that SA-ICPB could pump more electrons, implying the electronic interaction between CdS and microorganisms in the SA-ICPB system [55]. The conductive nanowires of MR-4 (Fig. 1c) also contributed. In summary, the photocatalytic oxidation, microbial metabolism, and electron interaction at the interface played a synergistic role in TCH degradation in SA-ICPB.

3.5. Degradation process and mechanism

In the SA-ICPB system, TCH was destroyed due to the attack of photocatalysis-produced ROS on the high electron density part of the TCH molecule, such as the double bond, phenolic hydroxyl, amine, and dimethylamino group [19]. Bacteria then utilized the product. By LC-MS analysis, three degradation pathways of TCH were deduced (Fig. 6).

Pathways 1 and 2 shared the same initial intermediate P2 ($m/z = 437.2$). Radical species attacked the lower energy N-C bond on C4 and the double bond on C6a-C7 of TCH (P1, $m/z = 445$) to generate P2. In pathway 1, the oxidation of P2 ($m/z = 437.2$) to a keto group can form P4 ($m/z = 432.2$), which was oxidized to P6 ($m/z = 401.3$). After that, some unique intermediates were identified before finally degrading to CO_2, H_2O, and inorganic ions. For example, P12 ($m/z = 242.1$) and P13 ($m/z = 235.1$) were only found under aerobic conditions, while P21 ($m/z = 131.2$), P22 ($m/z = 122.1$), and P23 ($m/z = 163.1$) were observed only under anaerobic conditions. In pathway 2, P2 was transformed to P4, P7 ($m/z = 393.2$), P8 ($m/z = 379.3$) and P9 ($m/z = 423.3$) through deamidation, deamination and hydroxylation. Subsequently, P16 ($m/z = 326.7$), P17 ($m/z = 340.2$), P18 ($m/z = 283.1$), P19 ($m/z = 318.1$), P20 ($m/z = 357.3$) were generated. These intermediates underwent hydroxylation, dealkylation, dehydration, ring opening and other reactions to produce P21, P22, P23, P24 ($m/z = 100.2$), and P25 ($m/z = 105.1$). During this process, P18, P21, P22, and P23 appeared only under anaerobic conditions.

In pathway 3, the C11A-C12 double bond of TCH was first attacked to form P3 ($m/z = 460.2$). The C2-C3 double bond was then attacked, generating P5 ($m/z = 476.2$). Afterward, the C6a-C7 double bond was oxidized, resulting in a ring-opening reaction to form P10 ($m/z = 525.2$). Subsequently, the methyl group at the C6 position and the amine methyl group at the C4 position were attacked, resulting in P14 ($m/z = 481.2$) and P15 ($m/z = 388.2$). P14 and P15 were further lysed or transformed to generate a series of low-molecule compounds (P21-P25) before being mineralized [30].

In summary, single photolysis and photocatalysis may mainly convert TCH into high molecule products (4-ring products, P2-P9) through hydroxylation, bond breaking, NH_3 and H_2O loss, and demethylation. Such a process cannot completely degrade such polycyclic chemicals, leaving intermediates for further treatment [21,33]. In this study, these 4-ring compounds were further destroyed by the synergistic effect of biological and photocatalytic degradation, generating P10-P25 before finally mineralizing. Notably, the intermediates species under aerobic conditions were fewer than anaerobic conditions. A possible explanation was that with oxygen as the acceptor of the biogenic electrons, aerobic respiration might lead to a different metabolism pathway than anaerobic degradation, where TCH and its degrading intermediates accept the electrons. Besides, oxygen in water may lead to increased ROS (e.g., $\cdot O_2^-$), accelerating organic degradation and producing different intermediates [39]. Furthermore, MR-4 grows and metabolizes faster aerobically [29]. Therefore, certain intermediates appearing in anaerobic conditions may not be produced or cannot be easily identified.

The current study realized the in-situ deposition of Cd^{2+} and S^{2-} through the metabolism of a representative electrochemical bacteria, *S. oneidensis* MR-4. Compared with other ICPB systems (Table S6), the SA-ICPB spontaneously loaded visible-light photocatalyst (bio-CdS) and biofilm onto the carriers (Fig. S7). In the SA-ICPB, AOP was combined with biodegradation without injuring bacterial metabolism but relived the biotoxicity of the pollutants towards microorganisms [26]. The organic binding of MR-4 with CdS is beneficial to the extracellular electron transfer process of bacteria (Fig. S6), which could have improved the microbial metabolism and the light energy utilization efficiency by the bio-CdS [28]. Due to the varied metabolism pathway of MR-4 and the changed internal effect of the bio-hybrid system, SA-ICPB

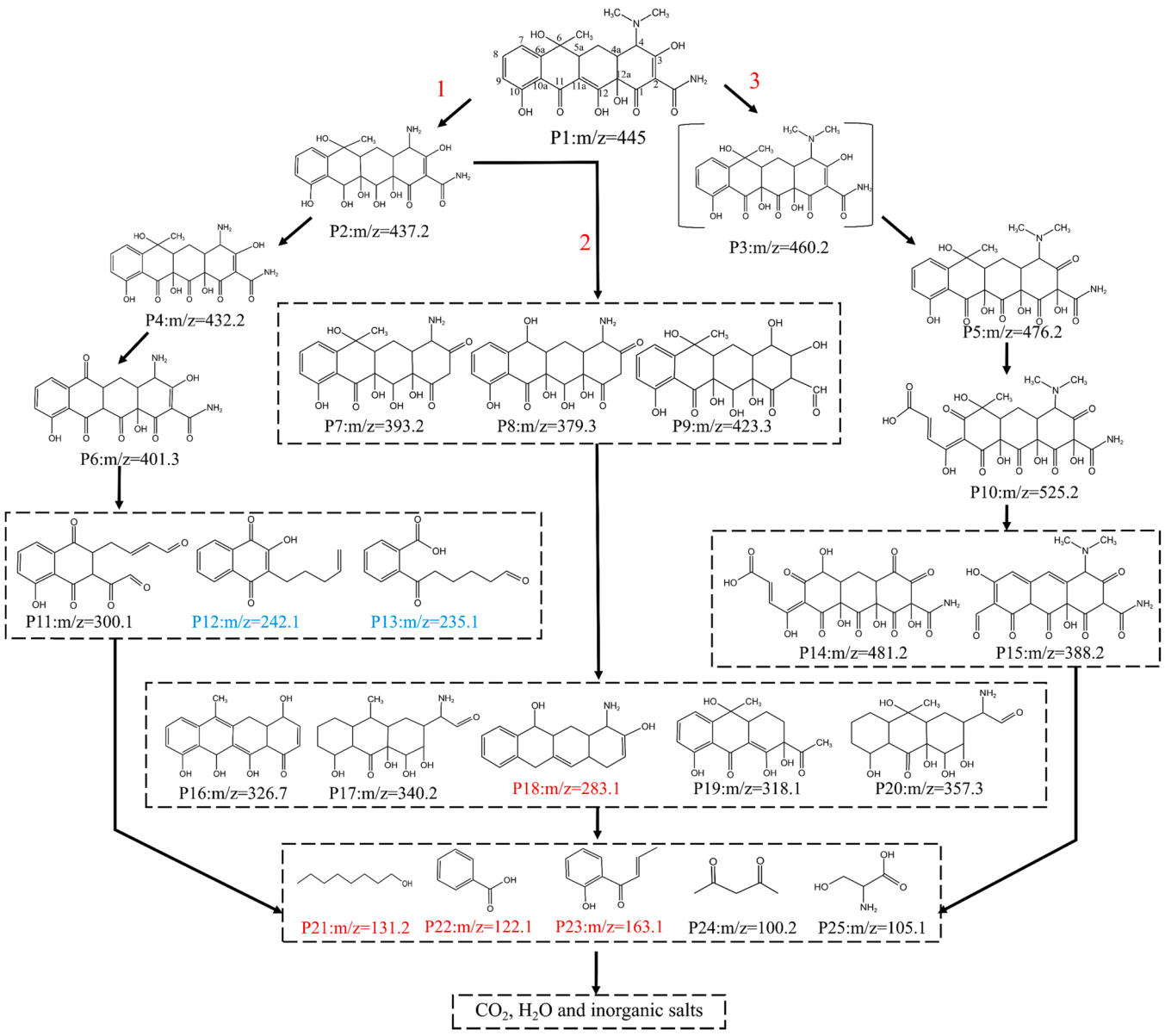

Fig. 6. Prediction of possible degradation pathways of TCH. Braces indicate products that are likely to be present but not detected; The *m/z* values marked in blue indicate the specific degradation intermediates under aerobic conditions. The *m/z* value marked in red indicates the specific degradation intermediates in the absence of oxygen.

showed a better performance for organic elimination with oxygen supply. The interaction of biogenerated nanomaterial with microbial cells under various circumstances should be explored for further development and application of such a bio-hybrid system.

4. Conclusion

Using microbial metabolism, SA-ICPB was spontaneously constructed for HMs recovery as sulfide photocatalysts and the deep degradation of antibiotics. SA-ICPB successfully combined biodegradation with photocatalytic degradation, providing a novel approach to eliminate such persistent antimicrobial organic pollutants. SA-ICPB can effectively remove TCH and COD under aerobic and anaerobic conditions through varied pathways, while better performance relies on oxygen participation. Photocatalysis effectively improved pollutants' biodegradability, overcoming the difficulty of biodegradation on antimicrobial substances. Biodegradation contributed to the intermediates' elimination, which was a drawback of photocatalysis. The synergistic effect of photocatalysis-biological degradation further improved efficiency. This study deepens the understanding of bacteria-photocatalyst interactions and the working mechanism of the biological-photocatalytic approach, which also expands the practical application of electrochemical bacteria in environmental remediation.

CRediT authorship contribution statement

Yu Wang: Conceptualization, Investigation, Writing – original draft. **Hang Qiu**: Investigation, Writing – review & editing. **Huan Niu:** Investigation, Writing – review & editing. **Hao Liu:** Data processing, Writing – review & editing. **Jinchang Liu:** Writing – review & editing. **Yinxue Jia**: Investigation, Writing – review & editing. **Haitao Ma:** Investigation, Writing – review & editing. **Likai Hao**: Funding acquisition, Writing – review & editing, Data processing. **Fei Xu**: Funding acquisition, Writing – review & editing, Data processing. **Zhongping Qiu**: Supervision and reviewing. **Can Wang:** Supervision and reviewing.

Declaration of Competing Interest

The authors declare that they have no known competing financial interests or personal relationships that could have appeared to influence the work reported in this paper.

Data Availability

Data will be made available on request.

Acknowledgments

This work was financially supported by the China Postdoctoral Science Foundation (2022M712630), the National Natural Science Foundation of China (No.51978576, 42207021, and 41877400), the Fundamental Research Funds for the Central Universities (2682021CX084, 2682022CX057), the Guizhou Provincial Department of Science and Technology (E2DF028), the National Key Research and Development Project of China (2018YFC1802601), the Startup Funding of the Chinese Academy of Sciences (2017–020), the Strategic Priority Research Program of Chinese Academy of Sciences (XDB40020300) and the State Key Laboratory of Environmental Geochemistry (SKLEG2018911), the Natural Science Foundation of Sichuan (2022NSFSC1670), the Science and technology project of Chengdu (2022-YF05–00269-SN and 2022-YF05–00909-SN), and the Large instrument and equipment open test fund of Southwest Jiaotong University (2022SRII-51). We thank Dr. Weizhen Fang of the Analysis & Testing center at Southwest Jiaotong University for the technical support. Thanks to Xingjia Ma at SCI-GO (www.sci-go.com) for the EPR analysis.

Environmental Implication

In this study, a self-assembled ICPB (SA-ICPB) was constructed using the electrochemical bacterium *S. oneidensis* MR-4 to remove cadmium (Cd) and tetracycline hydrochloride (TCH). Biogenerated CdS nanoparticles (Bio-CdS) coexist with bacterial cells on porous carriers to achieve the combination of photocatalysis and biodegradation. SA-ICPB can effectively remove TCH and COD through multiple pathways in both aerobic and anaerobic conditions. These results support the feasibility of SA-ICPB and the potential for simultaneous and efficient removal of HMs and antibiotics. The present study is expected to provide a new method for the advanced treatment of contaminated wastewater, whose development is significant.

Appendix A. Supporting information

Supplementary data associated with this article can be found in the online version at doi:10.1016/j.jhazmat.2023.131018.

References

[1] Bretschger, O., Obraztsova, A., Sturm, C.A., Chang, I.S., Gorby, Y.A., Reed, S.B., et al., 2008. Current production and metal oxide reduction by shewanella oneidensis MR-1 wild type and mutants. Appl Environ Microbiol 74 (2). https://doi.org/10.1128/aem.02560-07, 553-553.

[2] Budamagunta, V., Shameem, N., Irusappan, S., Parray, J.A., Thomas, M., Marimuthu, S., et al., 2023. Nanovesicle and extracellular polymeric substance synthesis from the remediation of heavy metal ions from soil. Environ Res 219, 114997. https://doi.org/10.1016/j.envres.2022.114997.

[3] Burdorf, L.D.W., Malkin, S.Y., Bjerg, J.T., van Rijswijk, P., Criens, F., Tramper, A., et al., 2018. The effect of oxygen availability on long-distance electron transport in marine sediments. Limnol Oceanogr 63 (4), 1799–1816. https://doi.org/10.1002/lno.10809.

[4] Cha, J., Carlson, K.H., 2019. Biodegradation of veterinary antibiotics in lagoon waters. Process Saf Environ Prot 127, 306–313. https://doi.org/10.1016/j.psep.2019.04.009.

[5] Chen, B., Lin, L., Fang, L., Yang, Y., Chen, E., Yuan, K., et al., 2018. Complex pollution of antibiotic resistance genes due to beta-lactam and aminoglycoside use in aquaculture farming. Water Res 134, 200–208. https://doi.org/10.1016/j.watres.2018.02.003.

[6] Chen, P., Zhang, T., Chen, Y., Ma, H., Wang, Y., Liu, W., et al., 2022. Integrated chamber-free microbial fuel cell for wastewater purification and bioenergy generation. Chem Eng J 442, 136091. https://doi.org/10.1016/j.cej.2022.136091.

[7] Chen, X., Liu, X., Zhu, L., Tao, X., Wang, X., 2022. One-step fabrication of novel MIL-53(Fe, Al) for synergistic adsorption-photocatalytic degradation of tetracycline. Chemosphere 291 (Pt 3), 133032. https://doi.org/10.1016/j.chemosphere.2021.133032.

[8] Chen, Z., Zhang, S., Liu, Y., Alharbi, N.S., Rabah, S.O., Wang, S., et al., 2020. Synthesis and fabrication of g-C_3N_4-based materials and their application in elimination of pollutants. Sci Total Environ 731, 139054. https://doi.org/10.1016/j.scitotenv.2020.139054.

[9] Ding, R., Yan, W., Wu, Y., Xiao, Y., Gang, H., Wang, S., et al., 2018. Light-excited photoelectrons coupled with bio-photocatalysis enhanced the degradation efficiency of oxytetracycline. Water Res 143, 589–598. https://doi.org/10.1016/j.watres.2018.06.068.

[10] Dold, B., 2014. Evolution of acid mine drainage formation in sulphidic mine tailings. Minerals 4 (3), 621–641. https://doi.org/10.3390/min4030621.

[11] Duan, B., Feng, Q., 2021. Comparison of the potential ecological and human health risks of heavy metals from sewage sludge and livestock manure for agricultural use. Toxics 9 (7), 145. https://doi.org/10.3390/toxics9070145.

[12] Felis, E., Buta-Hubeny, M., Zielinski, W., Hubeny, J., Harnisz, M., Bajkacz, S., et al., 2022. Solar-light driven photodegradation of antimicrobials, their transformation by-products and antibiotic resistance determinants in treated wastewater. Sci Total Environ 836, 155447. https://doi.org/10.1016/j.scitotenv.2022.155447.

[13] Feng, Z., Zhu, H., Deng, Q., He, Y., Li, J., Yin, J., et al., 2018. Environmental pollution induced by heavy metal(loid)s from pig farming. Environ Earth Sci 77 (3), 103. https://doi.org/10.1007/s12665-018-7300-2.

[14] Gu, D., Feng, Q., Guo, C., Hou, S., Lv, J., Zhang, Y., et al., 2019. Occurrence and risk assessment of antibiotics in manure, soil, wastewater, groundwater from livestock and poultry farms in Xuzhou, China. Bull Environ Contam Toxicol 103 (4), 590–596. https://doi.org/10.1007/s00128-019-02692-0.

[15] Han, H.X., Tian, L.J., Liu, D.F., Yu, H.Q., Sheng, G.P., Xiong, Y., 2022. Reversing electron transfer chain for light-driven hydrogen production in biotic-abiotic hybrid systems. J Am Chem Soc 144 (14), 6434–6441. https://doi.org/10.1021/jacs.2c00934.

[16] Hao, Y.M., Lou, S.Y., Zhou, S.M., Yuan, R.J., Zhu, G.Y., Li, N., 2012. Structural, optical, and magnetic studies of manganese-doped zinc oxide hierarchical microspheres by self-assembly of nanoparticles. Nanoscale Res Lett 7 (1), 100. https://doi.org/10.1186/1556-276X-7-100.

[17] Hong, M., Yu, L., Wang, Y., Zhang, J., Chen, Z., Dong, L., et al., 2019. Heavy metal adsorption with zeolites: the role of hierarchical pore architecture. Chem Eng J 359, 363–372. https://doi.org/10.1016/j.cej.2018.11.087.

[18] Hou, T., Liang, J., Wang, L., Zheng, Z., Wang, J., Xing, X., et al., 2021. $Cd_{1-x}Zn_xS$ biomineralized by engineered bacterium for efficient photocatalytic hydrogen production. Mater Today Energy 22, 100869. https://doi.org/10.1016/j.mtener.2021.100869.

[19] Jiang, H., Wang, Q., Chen, P., Zheng, H., Shi, J., Shu, H., et al., 2022. Photocatalytic degradation of tetracycline by using a regenerable (Bi)BiOBr/rGO composite. J Clean Prod 339, 130771. https://doi.org/10.1016/j.jclepro.2022.130771.

[20] Jiao, S., Zheng, S., Yin, D., Wang, L., Chen, L., 2008. Aqueous photolysis of tetracycline and toxicity of photolytic products to luminescent bacteria. Chemosphere 73 (3), 377–382. https://doi.org/10.1016/j.chemosphere.2008.05.042.

[21] Kaur, J., Pal, B., Singh, S., Kaur, H., 2023. Fabrication of highly efficient Au and layered double hydroxide modified g-C_3N_4 ternary composites for degradation of pharmaceutical drug: Pathways and mechanism. Surf Interfaces 36, 102583. https://doi.org/10.1016/j.surfin.2022.102583.

[22] Kim, J., Ahn, J., 2022. Emergence and spread of antibiotic-resistant foodborne pathogens from farm to table. Food Sci Biotechnol 31 (12), 1481–1499. https://doi.org/10.1007/s10068-022-01157-1.

[23] Kumar, P.S., Lakshmi Prabavathi, S., Indurani, P., Karuthapandian, S., Muthuraj, V., 2017. Light assisted synthesis of hierarchically structured Cu/CdS nanorods with superior photocatalytic activity, stability and photocatalytic mechanism. Sep Purif Technol 172, 192–201. https://doi.org/10.1016/j.seppur.2016.08.017.

[24] Lapo, B., Demey, H., Zapata, J., Romero, C., Sastre, A.M., 2018. Sorption of Hg(II) and Pb(II) Ions on Chitosan-Iron(III) from aqueous solutions: single and binary systems. Polym (Basel) 10 (4). https://doi.org/10.3390/polym10040367.

[25] Li, Y., Chen, L., Tian, X., Lin, L., Ding, R., Yan, W., et al., 2021. Functional role of mixed-culture microbe in photocatalysis coupled with biodegradation: Total organic carbon removal of ciprofloxacin. Sci Total Environ 784, 147049. https://doi.org/10.1016/j.scitotenv.2021.147049.

[26] Liang, Y., Jiao, C., Pan, L., Zhao, T., Liang, J., Xiong, J., et al., 2021. Degradation of chlorine dioxide bleaching wastewater and response of bacterial community in the intimately coupled system of visible-light photocatalysis and biodegradation. Environ Res 195, 110840. https://doi.org/10.1016/j.envres.2021.110840.

[27] Liang, Z., Wen, J., Zhou, Y., Liu, T., Dong, J., Zheng, W., et al., 2023. Comparative investigation of $BiOCl_{0.5}X_{0.5}$ (X = F, Br, and I) heterojunctions for solar-light driven photodegradation of tetracycline hydrochloride. Colloids Surf A: Physicochem Eng Asp 656, 130477. https://doi.org/10.1016/j.colsurfa.2022.130477.

[28] Liu, J., Liu, X., Ding, H., Ren, G., Sun, Y., Liu, Y., et al., 2021. Enhanced mechanism of extracellular electron transfer between semiconducting minerals anatase and

Pseudomonas aeruginosa PAO1 in euphotic zone. Bioelectrochemistry 141, 107849. https://doi.org/10.1016/j.bioelechem.2021.107849.
[29] Long, S., Yang, Y., Pavlostathis, S.G., Xiang, F., Sun, P., Li, N., et al., 2020. Toxicity of tetracycline and its transformation products to a phosphorus removing Shewanella strain. Chemosphere 246, 125681. https://doi.org/10.1016/j.chemosphere.2019.125681.
[30] Ma, Y., Xiong, H., Zhao, Z., Yu, Y., Zhou, D., Dong, S., 2018. Model-based evaluation of tetracycline hydrochloride removal and mineralization in an intimately coupled photocatalysis and biodegradation reactor. Chem Eng J 351, 967–975. https://doi.org/10.1016/j.cej.2018.06.167.
[31] Marsolek, M.D., Rittmann, B.E., 2016. Effect of substrate characteristics on microbial community structure, function, resistance, and resilience; application to coupled photocatalytic-biological treatment. Water Res 90, 1–8. https://doi.org/10.1016/j.watres.2015.12.002.
[32] Meitl, L.A., Eggleston, C.M., Colberg, P.J.S., Khare, N., Reardon, C.L., Shi, L., 2009. Electrochemical interaction of *Shewanella oneidensis* MR-1 and its outer membrane cytochromes OmcA and MtrC with hematite electrodes. Geochim Et Cosmochim Acta 73 (18), 5292–5307. https://doi.org/10.1016/j.gca.2009.06.021.
[33] Niu, J., Li, Y., Wang, W., 2013. Light-source-dependent role of nitrate and humic acid in tetracycline photolysis: kinetics and mechanism. Chemosphere 92 (11), 1423–1429. https://doi.org/10.1016/j.chemosphere.2013.03.049.
[34] Peng, A., Wang, C., Zhang, Z., Jin, X., Gu, C., Chen, Z., 2022. Tetracycline photolysis revisited: Overlooked day-night succession of the parent compound and metabolites in natural surface waters and associated ecotoxicity. Water Res 225, 119197. https://doi.org/10.1016/j.watres.2022.119197.
[35] Qin, Z., Zhao, Z., Jiao, W., Han, Z., Xia, L., Fang, Y., et al., 2020. Phenanthrene removal and response of bacterial community in the combined system of photocatalysis and PAH-degrading microbial consortium in laboratory system. Bioresour Technol 301, 122736. https://doi.org/10.1016/j.biortech.2020.122736.
[36] Qu, Z., Fang, L., Chen, D., Xu, H., Yan, N., 2017. Effective and regenerable Ag/graphene adsorbent for Hg(II) removal from aqueous solution. Fuel 203, 128–134. https://doi.org/10.1016/j.fuel.2017.04.105.
[37] Su, Z., Li, X., Xi, Y., Xie, T., Liu, Y., Liu, B., et al., 2022. Microbe-mediated transformation of metal sulfides: Mechanisms and environmental significance. Sci Total Environ 825, 153767. https://doi.org/10.1016/j.scitotenv.2022.153767.
[38] Suresh, A.K., Doktycz, M.J., Wang, W., Moon, J.W., Gu, B., Meyer 3rd, H.M., et al., 2011. Monodispersed biocompatible silver sulfide nanoparticles: facile extracellular biosynthesis using the gamma-proteobacterium, Shewanella oneidensis. Acta Biomater 7 (12), 4253–4258. https://doi.org/10.1016/j.actbio.2011.07.007.
[39] Tai, C., Zhang, S., Wang, J., Yin, Y., Shi, J., Wu, H., et al., 2017. Solar-induced generation of singlet oxygen and hydroxyl radical in sewage wastewaters. Environ Chem Lett 15 (3), 515–523. https://doi.org/10.1007/s10311-017-0625-3.
[40] Tiseo, K., Huber, L., Gilbert, M., Robinson, T.P., Van Boeckel, T.P., 2020. Global trends in antimicrobial use in food animals from 2017 to 2030. Antibiot (Basel) 9 (12), 918. https://doi.org/10.3390/antibiotics9120918.
[41] Tong, H., Zhan, X., Tian, X., Li, J., Qian, D., Wu, D., 2018. Understanding the energy level matching relationships between semiconductor photocatalysts and organic pollutants for effective photocatalytic degradations. J Colloid Interface Sci 526, 384–391. https://doi.org/10.1016/j.jcis.2018.05.009.
[42] Wang, C., Li, Y., Tan, H., Zhang, A., Xie, Y., Wu, B., et al., 2019. A novel microbe consortium, nano-visible light photocatalyst and microcapsule system to degrade PAHs. Chem Eng J 359, 1065–1074. https://doi.org/10.1016/j.cej.2018.11.077.
[43] Wang, X., Chen, Z., Kang, J., Zhao, X., Shen, J., 2018. Removal of tetracycline by aerobic granular sludge and its bacterial community dynamics in SBR. RSC Adv 8 (33), 18284–18293. https://doi.org/10.1039/c8ra01357h.
[44] Wang, X., Hu, J., Chen, Q., Zhang, P., Wu, L., Li, J., et al., 2019. Synergic degradation of 2,4,6-trichlorophenol in microbial fuel cells with intimately coupled photocatalytic-electrogenic anode. Water Res 156, 125–135. https://doi.org/10.1016/j.watres.2019.03.001.
[45] Wang, Y., Chen, C., Zhou, D., Xiong, H., Zhou, Y., Dong, S., et al., 2019. Eliminating partial-transformation products and mitigating residual toxicity of amoxicillin through intimately coupled photocatalysis and biodegradation. Chemosphere 237, 124491. https://doi.org/10.1016/j.chemosphere.2019.124491.
[46] Wu, G., Li, N., Mao, Y., Zhou, G., Gao, H., 2015. Endogenous generation of hydrogen sulfide and its regulation in Shewanella oneidensis. Front Microbiol 6 (1664–302X), 374. https://doi.org/10.3389/fmicb.2015.00374.
[47] Wu, S., Hu, H., Lin, Y., Zhang, J., Hu, Y.H., 2020. Visible light photocatalytic degradation of tetracycline over TiO_2. Chem Eng J 382, 122842. https://doi.org/10.1016/j.cej.2019.122842.
[48] Xiao, X., Han, X., Wang, L.-G., Long, F., Ma, X.-L., Xu, C.-C., et al., 2020. Anaerobically photoreductive degradation by CdS nanocrystal: biofabrication process and bioelectron-driven reaction coupled with Shewanella oneidensis MR-1. Biochem Eng J 154, 107466. https://doi.org/10.1016/j.bej.2019.107466.
[49] Xiao, X.X., Han, X., Wang, L.-G., Long, F., Ma, X.-L., Xu, C.-C., et al., 2020. Anaerobically photoreductive degradation by CdS nanocrystal: biofabrication process and bioelectron-driven reaction coupled with *Shewanella oneidensis* MR-1. Biochem Eng J 154. https://doi.org/10.1016/j.bej.2019.107466.
[50] Xiong, H., Zou, D., Zhou, D., Dong, S., Wang, J., Rittmann, B.E., 2017. Enhancing degradation and mineralization of tetracycline using intimately coupled photocatalysis and biodegradation (ICPB. Chem Eng J 316, 7–14. https://doi.org/10.1016/j.cej.2017.01.083.
[51] Xu, J., Luo, B., Gu, W., Jian, Y., Wu, F., Tang, Y., et al., 2018. Fabrication of In_2S_3/$NaTaO_3$ composites for enhancing the photocatalytic activity toward the degradation of tetracycline. N J Chem 42 (7), 5052–5058. https://doi.org/10.1039/c7nj05123a.
[52] Xu, Z., Gao, G., Pan, B., Zhang, W., Lv, L., 2015. A new combined process for efficient removal of Cu(II) organic complexes from wastewater: Fe(III) displacement/UV degradation/alkaline precipitation. Water Res 87, 378–384. https://doi.org/10.1016/j.watres.2015.09.025.
[53] Yang, Y., Zeng, Z., Zhang, C., Huang, D., Zeng, G., Xiao, R., et al., 2018. Construction of iodine vacancy-rich BiOI/Ag@AgI Z-scheme heterojunction photocatalysts for visible-light-driven tetracycline degradation: transformation pathways and mechanism insight. Chem Eng J 349, 808–821. https://doi.org/10.1016/j.cej.2018.05.093.
[54] Yu, C., Yu, L., Mohamed, A., Fang, J., Wu, Y., Dai, K., et al., 2022. Size-dependent visible-light-enhanced Cr(VI) bioreduction by hematite nanoparticles. Chemosphere 295, 133633. https://doi.org/10.1016/j.chemosphere.2022.133633.
[55] Yun, C.H., Kim, J., Hollmann, F., Park, C.B., 2022. Light-driven biocatalytic oxidation. Chem Sci 13 (42), 12260–12279. https://doi.org/10.1039/d2sc03483b.
[56] Zhang, S., Yi, J., Chen, J., Yin, Z., Tang, T., Wei, W., et al., 2020. Spatially confined Fe2O3 in hierarchical SiO2@TiO2 hollow sphere exhibiting superior photocatalytic efficiency for degrading antibiotics. Chem Eng J 380, 122583. https://doi.org/10.1016/j.cej.2019.122583.
[57] Zhao, D., Yu, Y., Chen, J.P., 2016. Treatment of lead contaminated water by a PVDF membrane that is modified by zirconium, phosphate and PVA. Water Res 101, 564–573. https://doi.org/10.1016/j.watres.2016.04.078.
[58] Zhou, L., Li, S., Li, F., 2022. Damage and elimination of soil and water antibiotic and heavy metal pollution caused by livestock husbandry. Environ Res 215 (Pt 2), 114188. https://doi.org/10.1016/j.envres.2022.114188.
[59] Zhou, X., Xi, H., Li, C., Dong, H., Wang, X., Zhao, Q., et al., 2021. Ultrasmall Ag species decorated on α-Fe_2O_3 nanorods toward high-efficient photocatalytic degrading tetracycline hydrochloride in water. J Chin Chem Soc 68 (6), 1013–1019. https://doi.org/10.1002/jccs.202000564.
[60] Zhu, Q., Sun, Y., Na, F., Wei, J., Xu, S., Li, Y., et al., 2019. Fabrication of CdS/titanium-oxo-cluster nanocomposites based on a Ti32 framework with enhanced photocatalytic activity for tetracycline hydrochloride degradation under visible light. Appl Catal B: Environ 254, 541–550. https://doi.org/10.1016/j.apcatb.2019.05.006.
[61] Zuo, W., Zhang, L., Zhang, Z., Tang, S., Sun, Y., Huang, H., et al., 2021. Degradation of organic pollutants by intimately coupling photocatalytic materials with microbes: a review. Crit Rev Biotechnol 41 (2), 273–299. https://doi.org/10.1080/07388551.2020.1869689.